Acta Mech 229, 2019–2039 (2018)
https://doi.org/10.1007/s00707-017-2085-z

ORIGINAL PAPER

Ali Triki

Dual-technique-based inline design strategy for water-hammer control in pressurized pipe flow

Received: 7 June 2017 / Revised: 30 October 2017 / Published online: 29 December 2017

Abstract A dual-technique-based inline strategy was investigated in this study as a sustainment to conventional-technique skills in terms of limitation of wave oscillation period spread-out. Instead of the single polymeric short section employed by the latter technique, the former is based on replacing an up- and downstream short section of the primitive piping system using another couple made of polymeric pipe-wall material. Numerical computations used the method of characteristics for the discretization of unconventional water-hammer model based on the Vitkovsky and the Kelvin–Voigt formulations. The efficiency of the dual technique was considered for two operating conditions associated with up- and downsurge frames. Moreover, two pipe-wall material types were utilized for short-section pipe wall, namely the HDPE or LDPE materials. Additionally, the conventional technique was also addressed in this study, for comparison purposes. First, analyses of pressure-head, circumferential-stress and radial-strain wave patterns, along with wave oscillation periods examination, confirmed that the dual technique could improve the efficiency of the conventional one, providing acceptable trade-off between the attenuation of pressure-head and circumferential-stress peaks (or crests), and limitation of period spreading and radial-strain amplification. Second, a parametric study of the sensitivity of the wave damping to the employed short-section dimensions was performed in terms of short-section length and diameter. This parametric study helped estimate the near-optimal values of the short-section dimensions.

Keywords Inline design strategy · Water hammer · Cavitating flow · HDPE–LDPE pipe-wall material · Method of characteristics · Vitkovsky formulation · Kelvin–Voigt formulation · Pressure head · Circumferential stress · Radial strain

List of symbols

A	Cross-sectional area of the pipe (m^2)
a_0	Elastic wave speed (m/s)
C_r	Courant number (–)
D	Main-pipe diameter (m)
$d_{\text{short-section}}$	Polymeric (sub-) short-section diameter (m)
E_0	Young's modulus of elasticity of the pipe wall (Pa)
e	Pipe-wall thickness (m)
f	Darcy–Weisbach friction factor (–)
g	Gravity acceleration (m/s^2)

A. Triki (✉)
Research Unit: Mechanics, Modelling Energy and Materials M2EM, National Engineering School of Gabes, University of Gabes, Zrig, 6029 Gabés, Tunisia
E-mail: ali.triki@enis.rnu.tn

h_f	Head loss per unit length (–)
$h = p/\gamma + z$	Pressure head (m)
$J_k = 1/E_k$	Instantaneous or elastic creep compliance (Pa^{-1})
K	Bulk modulus of elasticity of the fluid (Pa)
z	Elevation or pipe axis elevation (m)
k_v	Vitkovsky's unsteady decay coefficients (–)
L	Main steel-pipeline length (primitive system) (m)
$l_{\text{(sub-)short-section}}$	Polymeric (sub-) short-section length (m)
h^*	Absolute pressure head (Pa)
q	Average flowrate (m^3/s)
$R = f/2DA$	Pipeline resistance coefficient (–)
t	Time (s)
x	Coordinate along the pipe axis (m)
z	Elevation (m)

Greek symbols

α_0	Pressure-dependent volumetric ratio of gas in mixture (void fraction) (–)
α'	Dimensionless parameter (–)
Δt	Time-step increment (s)
Δx	Space-step increment (m)
ρ	Fluid density ($\mathrm{kg/m}^3$)
μ	Viscosity of the Kelvin–Voigt dashpot (m^2/s)
$\tau = \mu/E$	Retardation time for Kelvin–Voigt model (s)
ν'	Kinematic fluid viscosity (m^2/s)
ν	Poisson's ratio (–)
ψ	Numerical weighting factor (–)
θ	Relaxation coefficient for the local acceleration numerical scheme (–)
$\forall$	Volume of cavity (m^3)

Subscripts or Superscripts

0	Steady state
i	Section index
k	Kelvin–Voigt element index
ns	Number of sections
n_{kv}	Number of Kelvin–Voigt elements
g	Gas

Superscripts

j	Pipe index
k	Index of Kelvin–Voigt element
np	Number of pipes

1 Introduction

An effective design of industrial pressurized piping systems does require the adequate prevention of water-hammer surges associated with the rapid changes in internal fluid pressure and acceleration that occur in piping systems when the flow is suddenly interrupted, whether in normal setting maneuvers or in emergency cases [27,28]. Primarily, there are two different types of water-hammer surge waves, i.e., up- and downsurges, involving the increase or decrease of the wave amplitude, respectively. These surges may severely disturb the piping system operation and even damage the system parts. In more dramatic situations, these surges may experience more severe accidents such as pipe collapse, separation at bends as well as operator's fatalities,

whenever the cavitation onset was not anticipated in the design stage [5]. Physically, the latter phenomenon is characterized, first, by the disappearance of distributed void pockets throughout the flow system, due to the fluid local pressure drop to its gauge value. Subsequently, after reflections, the induced cavities collapse, leading to large pressure peaks [14].

Obviously, it is best wherever possible to avoid severe water-hammer surges. However, this is not always possible in most pipeline systems, and thus, the main functional design of the system should be modified to mitigate unacceptable conditions onset.

In this context, a large variety of design measures to control severe water-hammer surge impacts is considered by hydraulic designers. Briefly, these conventional measures may be sorted out into four major categories: (i) increasing pipeline pressure rating [1]; (ii) re-routing pipelines [16]; (iii) designing and installing surge control devices at the transient sensitive regions of the hydraulic system [6,29]; and (iv) implementing the operational control strategies of the hydraulic devices origin of the transient flow [1].

Fundamentally, the selection of the proper strategy depends upon the type of initiated surge event and varies from one hydraulic system to another. From a practical stand point, a combination of multiple techniques is the most desirable. Yet, despite technological development, substantial inconsistency between the used multiple devices may result in a worse condition at another location of the system due to the high complex nature of the nonlinear dynamic behaviors of the pipe network [17].

Recognizing these shortcomings, Massouh and Comolet [15] preemptively introduced the idea of adding a rubber short section to a steel piping system in order to mitigate excessive pressure rise due to a water-hammer event. Precisely, the experienced pipeline, considered by these authors, consists of a series connection of a rubber short section and a main steel pipe. The authors proved that such a technique could help in damping the excessive upsurge pressure rise. Indeed, the observed pressure-head behavior results in a gradually attenuated profile, accompanied with a long duration of wave oscillations.

Recently, basing on Massouh's proposals, Triki [23,24] explored the efficiency of an inline-based design strategy to upgrade existing steel piping systems faced to both up- and downsurge water-hammer severe effects. Precisely, the inline strategy, applied by the author, consists in replacing a short section of the transient sensitive regions of the existing piping system by another one made of polymeric pipe-wall material. Namely, the author made use of the high- and low-density polymeric materials (HDPE or LDPE). The author proved that such a technique could successfully be employed to attenuate excessive pressure-head rise and drop. However, the author noticed that such a strategy exhibited a fundamental drawback arising from the amplification of the wave oscillation period (spread-out), thus critically increasing the admissible duration for valve closure. The results showed a close dependence of the pressure-head attenuation on the waves phase speed. Specifically, the author observed that the case using an LDPE polymeric short section allowed a more important pressure-head damping and a larger period spread-out compared with the corresponding case employing an HDPE short section. Based on this result, it may be concluded that, as the wave speed of the short-section pipe-wall material decreases, the pressure-head attenuation and the wave oscillation period spread-out increase. Incidentally, these results have obvious physical explanations. Indeed, the reduced modulus and the viscoelastic mechanical behavior of plastic materials, used for the short-section pipe wall, result in a reduced wave speed (which may attenuate the surge wave amplitude) and a retarded hydraulic transient response (which may expand the wave fluctuation period) [7].

Accordingly, the main motivation for this research is to address the foregoing inline strategy drawback, involved by its primitive implementation technique. The practical idea, explored in this study, consists in the utilization of dual polymeric short sections instead of the single one employed in a previous configuration of the inline strategy, named hereby "conventional technique" [23]. More precisely, the proposed technique, called "dual technique," is based on replacing the short sections of the piping system, upstream each of its connections to the hydraulic system parts, by other ones made of HDPE or LDPE polymeric materials. This idea is intended to benefit simultaneously from the important pressure damping and the low period oscillation spread-out capacities provided by the former and the latter polymeric materials, respectively.

This paper is organized in six sections: the (1-D) Vitkovsky and the Kelvin–Voigt-based unconventional water-hammer model is next presented in Sect. 2; the transient flow computation, based on the method of characteristics (MOC) used for numerical computations, is detailed in Sect. 3; the result analyses and discussions obtained from the implementation of the proposed dual- technique-based inline strategy are presented in Sect. 4, as well as their counterpart issued from the conventional-technique configuration, being reported for comparison purposes. Ultimately, conclusions and recommendations for future work are provided in Sect. 5.

2 Materials and methods

Hydraulic transient modeling in pressurized pipe hydraulics relies commonly on classical water-hammer theories [22,30]. Yet, this model fails to accurately predict pressure wave damping associated with unsteady friction losses and pipe-wall material behavior embedded into real-world pipe systems. Among the various attempts to estimate the foregoing surge damping sources affecting water-hammer processes, the Vitkovsky et al. [26] and the Kelvin–Voigt formulations [13] embedded into the conventional water-hammer solver appear to be a promising approach, as it can accurately describe the entire design parameters such as pressure-head, circumferential-stress, and radial-strain behaviors. In particular, Covas et al. [8–10] used such an unconventional model to separately account for unsteady friction loss and pipe-wall viscoelastic behavior effects during water-hammer courses. The authors proved that such a combination could successfully reproduce experimental flow behaviors into polymeric pipe materials. Accordingly, this approach is selected for next transient flow predictions.

Shortly, the (1-D) unconventional water-hammer governing equations may be expressed as follows (detailed derivations are reported in [8]):

$$\frac{\partial h}{\partial t} + \frac{a_0^2}{gA}\frac{\partial q}{\partial x} + 2\frac{a_0^2}{g}\frac{\mathrm{d}\varepsilon_r}{\mathrm{d}t} = 0, \tag{1}$$

$$\frac{1}{A}\frac{\partial q}{\partial t} + g\frac{\partial h}{\partial x} + g\left(h_{f_s} + h_{f_u}\right) = 0 \tag{2}$$

where h is the pressure head, q is the flow discharge, A is the cross-sectional area of the pipe, g is the gravity acceleration, $a_0 = \sqrt{(K/\rho)/\{1 + \alpha\,(D/e)\,K\,J_0\}}$ is the wave speed, J_0 is the elastic creep compliance, α is a coefficient which relates to the pipe anchors' action ($\alpha = 1.07$, for thin wall elastic pipes [30]), h_{f_s} is the quasi-steady head-loss component per unit length evaluated by the Colebrook–White ($h_{f_s} = Rq\,|q|$) or the Hagen–Poiseuille rules ($h_{f_s} = 32\nu'\,|q|/\left(gD^2A\right)$), for turbulent or laminar flow regimes, respectively, h_{f_u} is the unsteady friction loss evaluated using the Vitkovsky et al. [26] formula: $h_{f_u} = (k_v/gA)\,\{(\partial q/\partial t) + a_0\mathrm{Sgn}\,(Q)\,|\partial q/\partial x|\}$, in which $k_v = 0.03$ is a decay coefficient and x and t are the coordinates along the pipe axis and time, respectively.

The retarded radial strain ε_r may be expressed using the linear-viscoelastic Kelvin–Voigt model (Fig. 1) [3]:

$$\varepsilon_r(x,t) = \sum_{k=1}^{N_{\mathrm{kv}}} \varepsilon_{rk} = \sum_{k=1}^{N_{\mathrm{kv}}} \frac{\alpha D}{2e}\rho g \int_0^s \left[h\,(x,t) - h_0\,(x)\right]\frac{J_k}{\tau_k}e^{-\frac{s}{\tau_k}}\,\mathrm{d}s \tag{3}$$

where J_k and τ_k ($k = 0 \cdots n_{\mathrm{kv}}$) denote the creep compliance, the retardation time coefficients associated with the springs and the dashpots of the kth Kelvin–Voigt element, respectively, n_{kv} is the number of Kelvin–Voigt elements, and h_0 designates the initial pressure-head value.

It is worth noting that the total radial strain indicated by Eq. (3) consists of elastic and viscous mechanical behavior parts, described by springs and dashpots exemplified in Fig. 1.

The circumferential stress can be computed as follows [30]:

$$\sigma = \frac{\alpha p D}{2e} \tag{4}$$

where p designates the pressure.

In the next section, the discretization steps of the unconventional water-hammer model using the MOC procedure are briefly presented. A detailed derivation of the general algorithm including viscoelasticity and unsteady friction within the conventional MOC solution is reported in, e.g., Soares et al. [20].

3 Calculations

The compatibility equations performed by the MOC procedure, using a rectangular mesh grid with a specified time step, corresponding to the discretization of Eqs. (1) and (2) along series pipeline parts, are given by [24,25]:

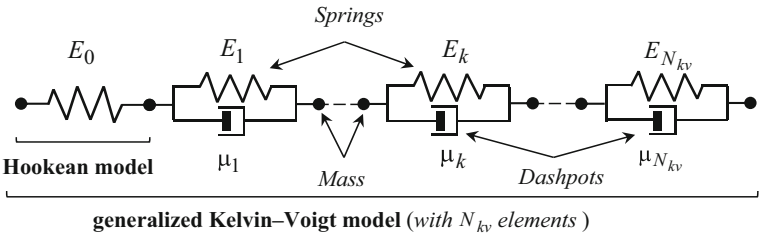

Fig. 1 Schematization of the generalized linear-viscoelastic Kelvin–Voigt model

$$\mathbf{C}^{j^{\pm}}: \frac{\mathrm{d}h}{\mathrm{d}t} \pm \frac{a_0^j}{g s^j}\frac{\mathrm{d}q}{\mathrm{d}t} + \frac{2a_0^2}{g}\left(\frac{\partial \varepsilon_r}{\mathrm{d}t}\right) \pm a_0^j h_f^j = 0 \quad \text{along} \quad \frac{\Delta x^j}{\Delta t} = \pm\frac{a_0^j}{c_r^j} \tag{5}$$

in which the superscript j refers to the pipe number ($1 \le j \le np$; np is the number of pipes), Δt denotes the time-step increment, and c_r designates the Courant number associated with the spatial discretization of the jth pipe.

Thereby, the unknown flow parameters can be straightforwardly integrated from Eq. (5) for each section i of the jth pipe ($1 \le i \le n_s^j$; n_s^j is the number of sections of the jth pipe) [20,25], as follows:

$$\mathbf{C}^{\pm}: \begin{cases} q_{i,t}^j = c_p^j - c_{a-}^j h_{i,t}^j \\ q_{i,t}^j = c_n^j + c_{a+}^j h_{i,t}^j \end{cases} \text{along} \quad \frac{\Delta x^j}{\Delta t} = \pm\frac{a_0^j}{c_r^j} \tag{6}$$

where

$$\begin{aligned}
c_p^j &= \left(q_{i-1,t-1}^j + \left(1/B^j\right) h_{i-1,t-\Delta t}^j + c_{p1}''^j + c_{p1}'''^j\right)/\left(1 + c'^j{}_{p} + c''^j{}_{p2} + c'''^j{}_{p2}\right);\\
B &= a_0/(gA);\\
c_n^j &= \left(q_{i+1,t-1}^j + \left(1/B^j\right) h_{i+1,t-\Delta t}^j + c''{}_{n1} + c_{n1}'''\right)/\left(1 + c_n'^j + c_{n2}''^j\right);\\
c_{a+}^j &= 1 + c_{p2}'''^j/\left(B^j\left(1 + c'^j{}_{p2} + c_{p2}''^j\right)\right);\\
c_p'^j &= R^j \Delta t \left|q_{i-1,t-1}^j\right|;\\
c_n'^j &= R^j \Delta t \left|q_{i+1,t-1}^j\right|;\\
R^j &= f^j/2D^j A^j;\\
c_{p1}''^j &= k_v\theta q_{i,t-1}^j - k_v(1-\theta)\left(q_{i-1,t-1}^j - q_{i-1,t-2}^j\right) - k_v \mathbf{sgn}\left(q_{i-1,t-1}^j\right)\left(q_{i,t-1}^j - q_{i-1,t-1}^j\right);\\
c_{n1}''^j &= k_v\theta q_{i,t-1}^j - k_v(1-\theta)\left(q_{i+1,t-1}^j - q_{i+1,t-2}^j\right) - k_v \mathbf{sgn}\left(q_{i+1,t-1}^j\right)\left(q_{i,t-1}^j - q_{i+1,t-1}^j\right);\\
c_{p2}''^j &= c_{n2}''^j = k_v\theta;
\end{aligned}$$

($\theta = 1$ is a relaxation coefficient); $c_{p1}'''^j = -c_{n1}'''^j = -2a_0^j A^j \Delta t \sum_{k=1}^{n_{kv}}\left[\varepsilon_{r_k}^j(x,t)/\partial t\right]$; $c_{p2}'''^j = c_{n2}'''^j = 2a_0^j A^j c_0 \gamma \sum_{k=1}^{n_{kv}} J_k^j\left(1 - e^{-(\Delta t/\tau_k)}\right)$; $\varepsilon_{r_{k,i,t-\Delta t}}^j = J_k^j c_0\left\{\left[h_{i,t-\Delta t}^j - h_{i,0}^j\right] - e^{-(\Delta t/\tau_k)}\left[h_{i,t-2\Delta t}^j - h_{i,0}^j\right] - \tau_k\left(1 - e^{-(\Delta t/\tau_k)}\right)\left[h_{i,t-\Delta t}^j - h_{i,t-2\Delta t}^j\right]/\Delta t\right\} + e^{-(\Delta t/\tau_k)}\varepsilon_{r_{k,i,t-2\Delta t}}$ and $c_0 = \alpha\gamma D^j/2e^j$.

It is worth noting that the above MOC procedure is established for a one-phase flow regime (i.e., without column separation). For a cavitating flow regime, the approximate flow solution may be achieved by including the discrete gas cavity model (DGCM) into the conventional MOC solution.

– *Discrete gas cavity model* Basically, the DGCM assumes that void cavities are lumped at the computing sections and a homogeneous distribution free gas mixture throughout the liquid. In addition, upon cavity formation at a computational section, a constant absolute pressure-head value, equal to the gauge pressure of the liquid (i.e., $h^* = h_g^*$), is imposed at this section.

The discretization of the perfect gas law for an isothermic evolution of each isolated gas cavity yields [30]:

$$\forall_{g_{i,t}}^{j}\left(h_{i,t}^{j}-z_{i}^{j}-h_{v}\right)=\left(h_{0}-z_{i}^{j}-h_{g}\right)\alpha_{0}A\Delta t \tag{7}$$

in which h_0 is the pressure-head reference, α_0 the void fraction at h_0, z_i^j the pipe axis elevation, and h_g the gauge pressure head of the liquid.
The cavity volume calculation is based on the discretization of the continuity equation applied for the cavity control volume [4]:

$$\forall_{g_{i,t}}^{j}=\forall_{g_{i,t-2\Delta t}}^{j}+\left[\psi\left(q_{d_{i,t}}^{j}-q_{u_{i,t}}^{j}\right)-(1-\psi)\left(q_{d_{i,t-2\Delta t}}^{j}-q_{u_{i,t-2\Delta t}}^{j}\right)\right] \tag{8}$$

where q_u and q_d are the flowrates, computed at the upstream and downstream sides of the cavity interface, using $\mathbf{C}^+$ and $\mathbf{C}^-$ characteristic equations (6), respectively, and ψ is a weighting factor, chosen in the range $0.5 \leq \psi \leq 1$ [4,30].
It is interesting to point out here that the flow regime is regarded as cavitating type for: $\forall_{g_{i,t}}^{j} \prec 0$. Otherwise, it is considered as a one-phase type.

– *Series connection of multi-pipes:* The flowrate and the pressure head at the series connection junction may be expressed, under no flow storage common hydraulic grade-line elevation assumptions, as follows [23,30]:

$$q_{ns^j,t}^{j-1}=q_{1,t}^{j} \quad \text{and} \quad h_{ns^j,t}^{j-1}=h_{1,t}^{j} \tag{9}$$

in which the right and left hands of Eq. (9) designate the hydraulic parameter values at the upstream and downstream sides of the junction section.

The final step to achieve numerical computations relates to the use of wave speed adjustment technique. This technique enables a common time-step Δt for the different pipes forming the hydraulic system [11,23,30]. This technique is based on slight adjustments to the original wave speed value such as $\tilde{a}_0^j = \left(1 \pm \eta^j\right) a_0^j$ (where η^j is a permissible wave speed variation of the jth pipe ($\eta^j \leq 0.01$)), to match an even integer value for the section number n_s^j satisfying: $n_s^j = L^j / \left(\tilde{a}_0^j \Delta t\right)$ [30].

4 Model validation

In order to ensure the performance of the developed numerical model in capturing the pressure surge behavior in a polymeric piping system, the experimental measurements carried out by Covas et al. [8] on a reservoir-pipe-valve system were used. The reservoir head at the upstream end of the system was fixed at $H_0 = 35$ m, and the valve at the downstream end was initially fully open. The diameter and length of the HDPE piping system were: $L = 270$ m and $D = 50.6$ mm, respectively. The creep compliance coefficients of the generalized Kelvin–Voigt model, associated with the creep behavior of the HDPE pipe-wall material are reported in Table 1 [8]. The steady-state flowrate in the pipeline was $Q_0 = 1.008$ l/s, and the transient signal resulted from the instantaneous and complete closure of the downstream valve.

Figure 2 compares the computed and measured pressure head at the downstream valve section. Specifically, numerical results are obtained basing on the unconventional water-hammer model using the Vitkovsky unsteady friction formulation, with and without considering the viscoelastic behavior of the pipe wall.
Figure 2 clearly illustrates that the proposed numerical model, accounting for unsteady friction and viscoelasticity, correctly replicates the magnitude and the phase shift of the resulting water-hammer pressure wave, for the first cycle of pressure-head oscillation. However, the numerical results, accounting only for the unsteady friction, illustrate important discrepancies between measured and numerical results in terms of amplitude, period, and shape of the pressure wave oscillation patterns.

Moreover, Fig. 2 reveals another remarkable feature regarding viscoelastic and unsteady friction factors. Indeed, these factors have comparable effects on the attenuation of the transient during its initial stage. However, as time increases, the viscoelastic effect dominates the attenuation of the transient in its latter stages. Furthermore, a faster decay of the transient pressure is observed when considering the viscoelastic effect,

Table 1 Specification of creep compliance coefficients for the employed pipe-wall materials

Pipe-wall materials	J_0 (GPa^{-1})	J_1 (GPa^{-1})	τ_1(s)	J_2 (GPa^{-1})	τ_2 (s)	J_3 (GPa^{-1})	τ_3 (s)	J_4 (GPa^{-1})	τ_4(s)	J_5 (GPa^{-1})	τ_5 (s)
Steel	0.0049	–		–		–		–		–	–
HDPE	0.8032	1.057	0.05	1.054	0.5	0.905	1.5	0.262	5.0	0.746	10.0
LDPE	2.0830	7.54	0.000089	10.46	0.022	12.37	1.864	–	–	–	–

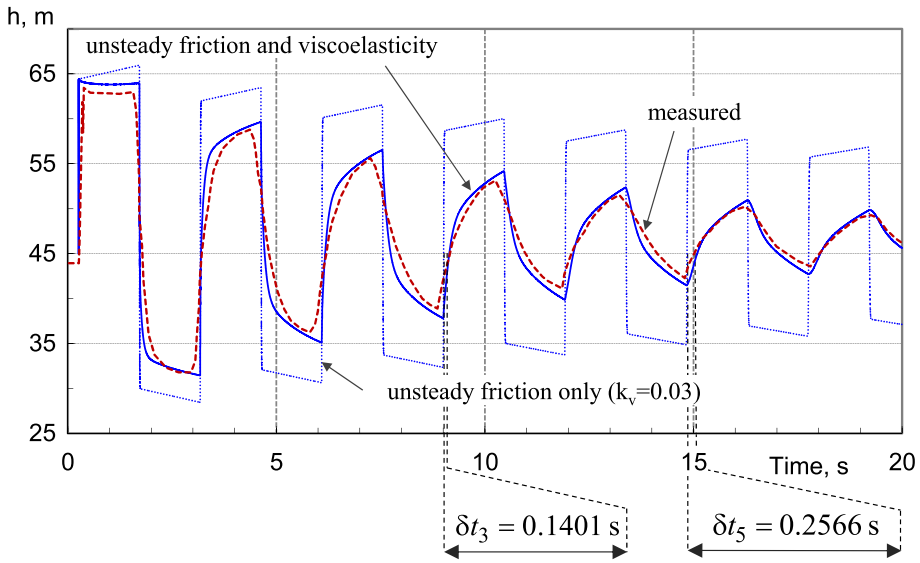

Fig. 2 Comparison of computed and measured pressure heads at the downstream valve section (x = 270 m)

which is mainly attributed to the time shift between the pressure response and the retarded strain response [18].

On the other hand, Fig. 2 illustrates that the pressure attenuation is accompanied with an increasing spreading of the wave oscillation period; for example, the retardation time values observed for the 3rd and the 5th period are: $\delta t_3 = 0.1401$ s and $\delta t_5 = 0.2566$ s, respectively. This mechanism is due to the correlation between the retardation time, which increases with time, and the period of wave oscillations [18].

5 Applications, results, and discussion

This section is devoted to the study of the effectiveness of the dual-technique-based inline strategy targeting to improve the competitiveness of the conventional-technique-based one, with respect to the limitation of the excessive spread-out of wave oscillation period. First, it may be helpful to briefly revisit the conventional- and the dual-technique concepts. As mentioned earlier, the latter technique is conceptualized upon the conventional one. More precisely, the conventional-technique concept is based on the replacement of a short section of the main steel-pipeline sensitive region by another one made of polymeric pipe-wall material. However, the dual technique consists in applying the same handling, but at each connection of the main steel pipeline to other hydraulic parts, using dual polymeric sub-short sections.

In the following, up- and downsurge initiated water-hammer event types are separately investigated in the next two subsections. In each case, the results associated with the conventional-technique-based inline strategy are also addressed, for comparison purposes. It is noteworthy here that the short-section length used in the conventional technique is equally split into two sub-short section lengths used in the dual-technique configuration. It has been proceeded in such a way in order to target a consistent comparison between the two foregoing techniques with regard to the volume of polymeric pipe-wall materials used in each technique (i.e., conventional and dual techniques). In addition, the next investigations employ the HDPE and the LDPE polymeric pipe-wall material types for the (sub- or) short-section pipe wall. Therewith, four configurations of the dual-technique-based controlled system are involved by the different combinations of the utilized sub-

short-section material types. Specifically, these combinations include (HDPE and HDPE); (LDPE and LDPE); (HDPE and LDPE); or (LDPE and HDPE) sub-short sections (in the aforementioned abbreviations, the first and second notation terms designate the material types of the up- and downstream short section, respectively).

The generalized Kelvin–Voigt coefficients associated with the linear-viscoelastic behavior of the employed HDPE and LDPE materials are listed in Table 1 [8,13], respectively). The following water-hammer calculations were performed by a MOC-based algorithm, using a specified time step.

Note that the next interpretations use the following definitions: $\delta x^{\text{dual-technique}}_{\text{up-surge/down-surge}} = x^{\text{dual-technique}}_{\text{max/min}} - x^{Steel}_{\text{max/min}}$; $\delta' x^{\text{dual-technique}}_{\text{up-surge/down-surge}} = x^{\text{dual-technique}}_{\text{max/min}} - x^{\text{HDPE}}_{\text{max/min}}$ and $\delta'' x^{\text{dual-technique}}_{\text{up-surge/down-surge}} = x^{\text{dual-technique}}_{\text{max/min}} - x^{\text{LDPE}}_{\text{max/min}}$, where x denotes the wave features: $\{h\,;\,\sigma$ or $\varepsilon\}$. Likewise, the pressure-head amortization rates are calculated using the following relations: $\eta^{\text{dual-technique}}_{\text{up-surge/down-surge}} = \left(h^{\text{dual-technique}}_{\text{max/min}} - h^{\text{Steel}}_{\text{max/min}}\right)/h^{\text{Steel}}_{\text{max/min}}$; $\eta'^{\text{dual-technique}}_{\text{up-surge/down-surge}} = \left(h^{\text{dual-technique}}_{\text{max/min}} - h^{\text{HDPE-conventional-technique}}_{\text{max/min}}\right)/h^{\text{HDPE-conventional-technique}}_{\text{max/min}}$ and $\eta''^{\text{dual-technique}}_{\text{up-surge/down-surge}} = \left(h^{\text{dual-technique}}_{\text{max/min}} - h^{\text{LDPE-conventionaltechnique}}_{\text{max/min}}\right)/h^{\text{LDPE-conventional-technique}}_{\text{max/min}}$. Similar notations are employed for evaluating the phase shift between the first cycle of wave oscillations. For example, the phase shift between the first cycle of wave oscillations involved by the dual-technique-based controlled system and their counterpart predicted for the primitive system or the controlled system using HDPE or LDPE conventional techniques are evaluated as follows: $\delta T^{\text{dual-technique}}_{\text{1st cycle}} = \left|T^{\text{dual-technique}}_{\text{1st cycle}} - T^{\text{Steel}}_{\text{1st cycle}}\right|$; $\delta' T^{\text{dual-technique}}_{1^{\text{st}}\text{cycle}} = \left|T^{\text{dual-technique}}_{\text{1st cycle}} - T^{\text{HDPE}}_{1^{\text{st}}\text{cycle}}\right|$; $\delta'' T^{\text{dual-technique}}_{\text{1st cycle}} = \left|T^{\text{dual-technique}}_{\text{1st cycle}} - T^{\text{LDPE}}_{\text{1st cycle}}\right|$.

5.1 Water-hammer upsurge event case

To assess the reliability of the proposed control technique with regard to water-hammer upsurge maneuver, investigations are carried out on a reservoir-pipe-valve system, sketched in Fig. 3a (primitive system). The piping system specifications are: $L = 143.7$ m; $D = 50.6$ mm; $e = 3.35$ mm; and $a_0 = 1369.7$ m/s. The initial steady-state flowrate and downstream pressure head correspond to: $q_0 = 0.58$l/s and $h_{0|valve} = 45$ m, respectively. The transient water-hammer upsurges arise from the abrupt and full switch-off of the downstream valve. Such a transient event is subjected to the following boundary conditions:

$$q_{|x=L} = 0 \text{ and } h_{|x=0} = h_{0|\text{reservoir}}\,(t \succ 0). \tag{10}$$

For this specific water-hammer event, the conventional-technique- based inline strategy consists in replacing a downstream short section of the existing piping system by another one made of polymeric materials. However, the dual-technique-based one is implemented by modifying the piping system, using the same handling of the hydraulic system, but at its up- and downstream extremities (Fig. 3b).

As a first investigation step, the short-section length and diameter, employed within the conventional-technique frame, are set equal to: $l^{\text{conventional}}_{\text{short-section}} = 5$ m and $d^{\text{conventional}}_{\text{short-section}}\,(= D) = 50.6$ mm, respectively. Thereupon, the sub-short-section lengths and diameters, used within the dual-technique frame, correspond to: $l^{\text{dual}}_{\text{sub-shortsection}} = \left(l^{\text{conventional}}_{\text{short-section}}/2\right) = 2.5$ m and $d^{\text{dual}}_{\text{sub-shortsection}}\left(= d^{\text{conventional}}_{\text{short-section}}\right) = 50.6$ mm, respectively. It is worth noting that the steel-pipe length of the controlled systems (i.e., using the conventional or the dual technique) is reduced to the value: $l_{\text{main-pipe}}\left(= L - l^{\text{conventional}}_{\text{short-section}} = L - 2 \times l^{\text{compound}}_{\text{sub-shortsection}}\right) = 138.7$ m, while it was equal to: $L = 143.7$ m in the primitive system (i.e., uncontrolled system).

The MOC algorithm applied herein, for numerical computations, uses a specified time interval $\left\{\Delta t = 4.49 \times 10^{-3}\text{ s}\right\}$ and Courant number values set: {0.97694; 0.71354; and 1}, associated with the discretization of the steel pipe along with the HDPE and LDPE polymeric sub-short-section domains, respectively.

Figure 4a–c, respectively, displays the downstream pressure heads, circumferential stresses, and radial strains versus time predicted for the primitive hydraulic system, along with the corresponding curves involved in the controlled systems using the dual or the conventional technique. Specifically, the (HDPE–HDPE), (LDPE–LDPE), (HDPE–LDPE) or (LDPE–HDPE) combinations of sub-short-section materials are performed for the controlled system utilizing the dual technique. However, the HDPE or LDPE short-section setups are addressed for the controlled system based on the conventional technique. In addition, the main features of the wave patterns, displayed in Fig. 4a–c, are detailed in Table 2a–d, respectively.

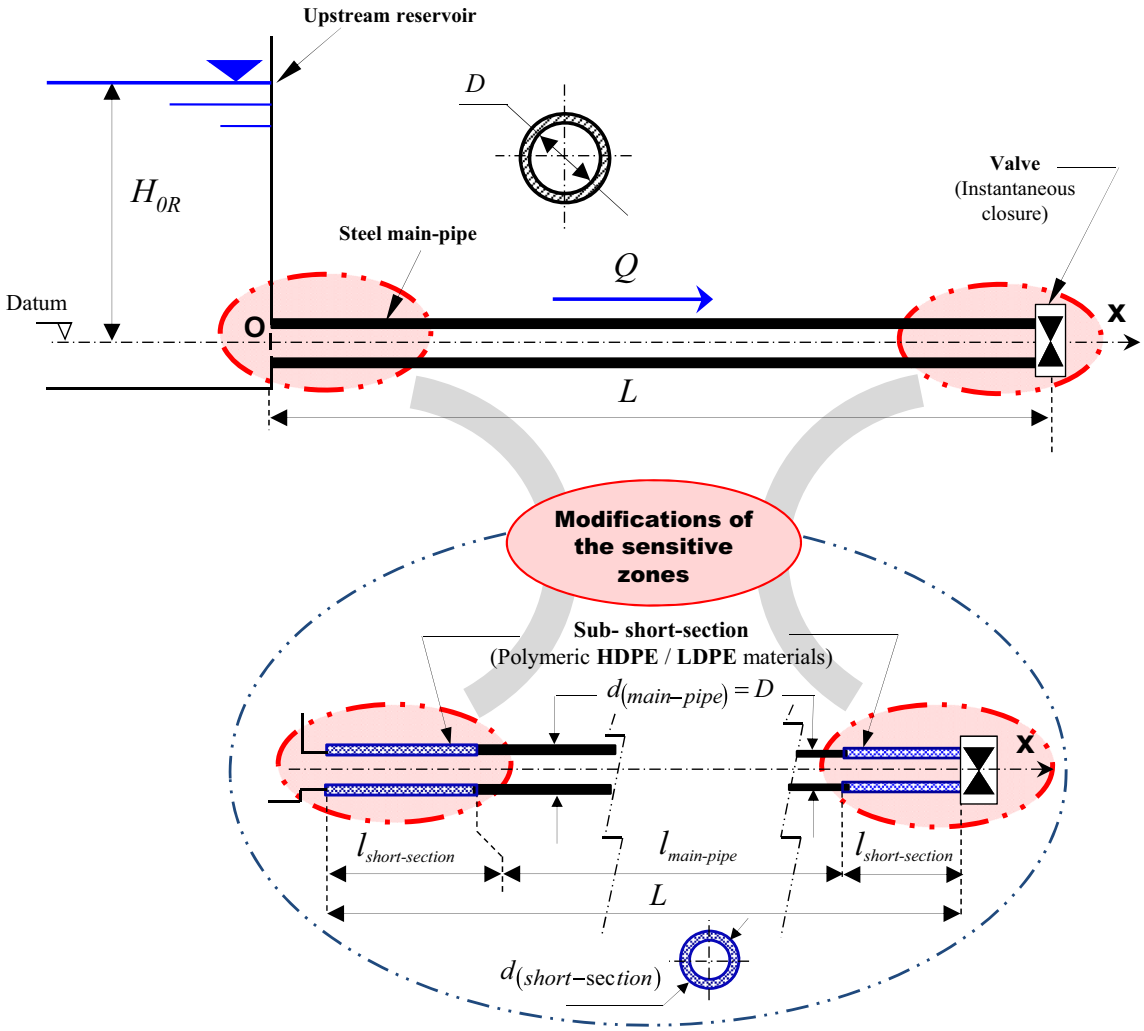

Fig. 3 Schematic layouts of: **a** primitive (non-controlled) system; **b** controlled system using the dual-technique-based inline strategy, for the upsurge control test case

At first glance, it is clear that Fig. 4a–c displays five wave pattern groups associated with the (i) primitive system (blue-dotted line), dual-technique-based controlled systems using (ii) HDPE and (iii) LDPE setups, dual-technique-based controlled systems using (iv) HDPE–HDPE or LDPE–HDPE (brown or blue solid lines), and (v) LDPE–LDPE or HDPE–LDPE setups (pink or green solid lines).

Based on the data shown in Fig. 4a–c (together with Table 2a–d), the following interpretation may be given for the first cycle of wave oscillation:

First, Fig. 4a, b illustrates an excessive rise of pressure head and circumferential stress observed in the primitive system case, succeeding the downstream valve closure maneuver. In this condition, the magnitude values of pressure head and circumferential-stress upsurges are: $\Delta h^{\text{steel-pipe}}_{\text{up-surge}} = 40.6$ m and $\Delta\sigma^{\text{steel-pipe}}_{\text{up-surge}} = 3.22$ MPa, respectively. Nonetheless, Fig. 4c (zoomed panel) shows a very small upsurge amplification of the radial strain magnitude: $\Delta\varepsilon^{\text{steel-pipe}}_{\text{up-surge}} = 26\ \mu\text{m/m}$.

Second, the wave pattern associated with the dual technique using HDPE–HDPE short sections or LDPE–HDPE sub-short sections is practically undistinguishable during the first cycle of wave oscillations. Furthermore, these controlled system setups have no observable contribution to the wave damping. Thus, these dual-technique setups are ruled out from further interpretation.

Third, similarly to the foregoing case, the configurations based on the dual-technique group, using HDPE–LDPE or LDPE–LDPE sub-short sections, display slightly distinguishable profile evolutions. Likewise, a substantial surge damping is depicted in these cases compared with the primitive system case. Thus, these

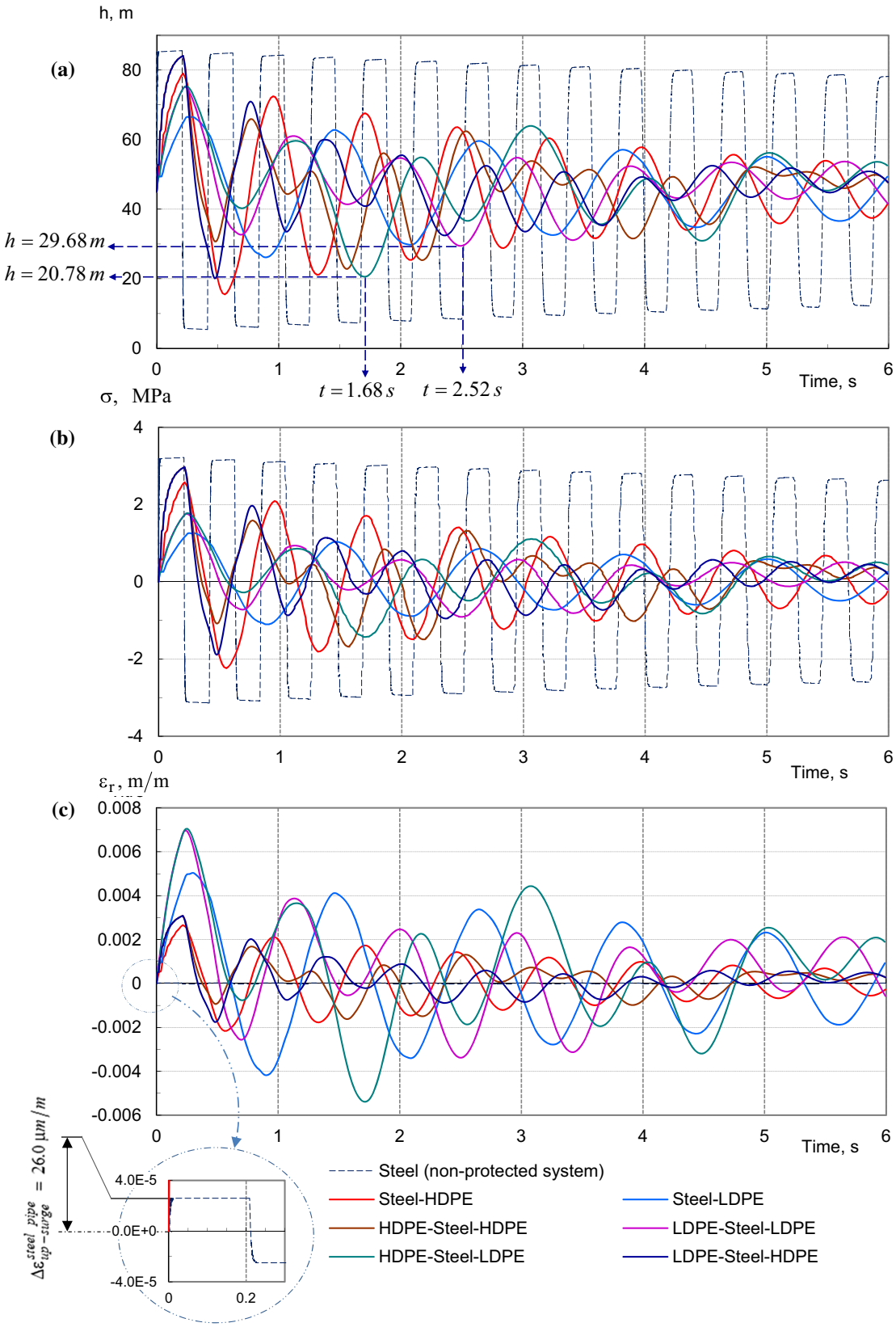

Fig. 4 Comparison of downstream **a** pressure heads, **b** circumferential stresses, and **c** radial strains versus time for the hydraulic system with and without implementation of the protection procedure

Table 2 Summary of the first cycle water-hammer wave characteristics in Fig. 4

Parameters		Steel main pipe (Non-controlled system)	Upstream short section (Conventional technique)		Up- and downstream sub-short sections (Dual technique)			
			HDPE	LDPE	HDPE–HDPE	LDPE–LDPE	HDPE–LDPE	LDPE–HDPE
(a) Pressure heads								
h_{max}	(m)	85.6	79.0	66.6	84.1	75.1	75.4	84.1
h_{min}	(m)	5.4	15.5	26.1	22.8	29.5	20.6	20.1
$\Delta h_{\text{up-surge}}$	(m)	40.6	34.0	21.6	39.1	30.1	30.4	39.1
$\delta h_{\text{up-surge}}$	(m)	–	6.55	19.01	1.47	10.45	10.19	1.47
$\delta' h_{\text{up-surge}}$	(m)	–	–	–	5.08	3.90	3.64	5.08
$\delta'' h_{\text{up-surge}}$	(m)	–	–	–	17.54	8.56	8.83	17.54
$\eta h_{\text{up-surge}}$	(%)	–	16.14	46.84	3.63	25.75	25.10	3.63
$\eta' h_{\text{up-surge}}$	(%)	–	–	–	14.92	11.46	10.68	14.92
$\eta'' h_{\text{up-surge}}$	(%)	–	–	–	81.29	39.68	40.90	81.29
(b) Circumferential-stress								
$\Delta\sigma_{\text{up-surge}}$	(MPa)	3.22	2.58	1.26	2.97	1.76	1.78	2.97
$\delta\sigma_{\text{up-surge}}$	(MPa)	–	0.64	1.96	0.25	1.46	1.44	0.25
$\delta'\sigma_{\text{up-surge}}$	(MPa)	–	–	–	0.39	− 0.82	− 0.80	0.39
$\delta''\sigma_{\text{up-surge}}$	(MPa)	–	–	–	1.71	0.50	0.52	1.71
$\eta\sigma_{\text{up-surge}}$	(%)	–	19.81	60.82	7.84	45.27	44.79	7.84
$\eta'\sigma_{\text{up-surge}}$	(%)	–	–	–	14.92	− 31.75	− 31.15	14.92
$\eta''\sigma_{\text{up-surge}}$	(%)	–	–	–	135.19	39.68	40.90	135.19
(c) Radial strain								
$\Delta\varepsilon_{\text{up-surge}}$	(mm/m)	26.6×10^{-3}	2.66	5.04	3.09	6.97	7.05	3.09
$\delta\varepsilon_{\text{up-surge}}$	(mm/m)	–	2.63	5.01	3.06	6.94	7.02	3.06
$\delta'\varepsilon_{\text{up-surge}}$	(mm/m)	–	–	–	0.43	4.31	4.39	0.43
$\delta''\varepsilon_{\text{up-surge}}$	(mm/m)	–	–	–	− 1.95	1.93	2.01	− 1.95
$\eta'\varepsilon_{\text{up-surge}}$	(%)	–	–	–	16.01	161.99	164.95	16.01
$\eta''\varepsilon_{\text{up-surge}}$	(%)	–	–	–	− 38.74	38.34	39.91	− 38.74
(d) Period								
T	(s)	0.42	0.756	1.18	0.63	0.918	0.876	0.612
δT	(s)	–	0.336	0.76	0.21	0.498	0.456	0.192
$\delta' T$	(s)	–	–	0.424	0.126	0.162	0.12	0.162
$\delta'' T$	(s)	–	–	–	0.55	0.262	0.304	0.568

cases deserve further interpretation. Precisely, referring to Fig.4a and Table 2a, the pressure-head upsurge magnitude values, calculated for these controlled system cases (i.e., using HDPE–LDPE or LDPE– LDPE sub-short sections), are: $\Delta h_{\text{up-surge}}^{\text{HDPE-LDPE}} = 30.4$ m or $\Delta h_{\text{up-surge}}^{\text{LDPE-LDPE}} = 30.1$ m, respectively. Compared with the flow pattern of the primitive system case, these configurations allow pressure-head attenuations equal to: $\delta h_{\text{up-surge}}^{\text{HDPE-LDPE}} = 10.2$ m or $\delta h_{\text{up-surge}}^{\text{LDPE-LDPE}} = 10.5$ m, respectively. In return, the pressure-head amortization rates provided by HDPE–LDPE or LDPE–LDPE sub-short-section-based layouts, compared with the primitive system one, are about: $\eta_{\text{up-surge}}^{\text{HDPE-LDPE}} = 25.75\%$ or $\eta_{\text{up-surge}}^{\text{LDPE-LDPE}} = 25.10\%$. On the other hand, the dual-technique setups discussed herein allow larger pressure-head attenuations compared with HDPE-based conventional technique: $\delta' h_{\text{up-surge}}^{\text{HDPE-LDPE}} = 3.6$ m or $\delta' h_{\text{up-surge}}^{\text{LDPE-LDPE}} = 3.9$ m. Thereupon, the pressure-head amortization rates provided by the dual-technique setups are about: $\eta'^{\text{HDPE-LDPE}}_{\text{up-surge}} = 10.68\%$ or $\eta'^{\text{LDPE-LDPE}}_{\text{up-surge}} = 11.46\%$, relatively to those of the HDPE-based conventional technique. Contrarily, the upsurge pressure-head magnitude performed by the dual-technique setups, discussed herein, is more important than those provided by the LDPE-based conventional technique: $\delta h''^{\text{HDPE-LDPE}}_{\text{up-surge}} = 8.8$ m or $\delta h''^{\text{LDPE-LDPE}}_{\text{up-surge}} = 8.6$ m. More precisely, the pressure-head amortization rates provided by HDPE–LDPE or LDPE–LDPE sub-short-section-based layouts, relative to those of the primitive system, are about: $\eta''^{\text{HDPE-LDPE}}_{\text{up-surge}} = 40.90\%$ or $\eta''^{\text{LDPE-LDPE}}_{\text{up-surge}} = 39.68\%$.

Similar interpretations may be given for the circumferential-stress pattern plotted in Fig. 4b. However, inverse comments may be addressed with respect to the radial-strain pattern plotted in Fig. 4c (and Table 2c). Indeed, a similar comparison procedure indicates that the dual-technique setups, discussed above (i.e., based on HDPE–LDPE or LDPE–LDPE sub-short sections), lead to an amplification of radial strain larger than their counterparts involved by the conventional one employing an HDPE short-section $\delta' \varepsilon_{\text{up-surge}}^{\text{HDPE-LDPE}} = 4.39$ mm/m or $\delta' \varepsilon_{\text{up-surge}}^{\text{LDPE-LDPE}} = 4.31$ mm/m. However, the dual-technique setups yield better results (i.e.,

lower amplification of radial strain) as compared with the conventional technique utilizing an LDPE short-section ($\delta\varepsilon''^{\text{HDPE-LDPE}}_{\text{up-surge}} = 2.01$ mm/m or $\delta\varepsilon''^{\text{LDPE-LDPE}}_{\text{up-surge}} = 1.93$ mm/m). Incidentally, one recalls that a very small upsurge magnitude of radial strain is observed for the primitive system case (i.e., steel pipe): $\Delta\varepsilon^{\text{steel-pipe}}_{\text{up-surge}} = 26.0\ \mu$m/m.

Fourth, basing on Fig. 4 and Table 2d, it can be inferred that a remarkable spread-out of wave oscillation periods is induced by the inline strategy based on either dual or conventional technique. In particular, the phase shifts observed between HDPE–LDPE and LDPE–LDPE dual-technique setups and the primitive system case are equal to: $\delta T^{\text{HDPE-LDPE}}_{\text{1st cycle}} = 0.498$ s or $\delta T^{\text{LDPE-LDPE}}_{\text{1st cycle}} = 0.456$ s, respectively. Similar interpretations can be made, but lower phase shifts are deduced for the foregoing dual-technique cases as compared with the conventional one based on HDPE short section: $\delta' T^{\text{HDPE-LDPE}}_{\text{1st cycle}} = 0.12$ s or $\delta' T^{\text{LDPE-LDPE}}_{\text{1st cycle}} = 0.162$ s. However, the considered dual techniques allow an important limitation of period spread-out as compared with that involved by the LDPE-based conventional technique: $\delta'' T^{\text{HDPE-LDPE}}_{\text{1st cycle}} = 0.304$ s or $\delta'' T^{\text{LDPE-LDPE}}_{\text{1st cycle}} = 0.262$ s.

Specifically, referring to Table 2d, the phase shift observed between the dual and the conventional technique employing an HDPE (sub-) short section is equal to: $\delta' T^{\text{HDPE-HDPE}}_{\text{1st cycle}} = 0.126$ s. A much more important value of phase shift is observed for the cases utilizing a LDPE (sub-) short section ($\delta'' T^{\text{LDPE-LDPE}}_{\text{1st cycle}} = 0.126$ s).

From the above result interpretations, it is believed that the HDPE–LDPE or LDPE–LDPE setups of the dual technique provide a satisfactory trade-off between the damping of pressure head and circumferential stress on the one hand, and limitation of period spreading and radial-strain amplification on the other hand. Moreover, it is interesting to point out herein that the latter configuration (i.e., LDPE–LDPE) displays better results with respect to pressure-head decrease. For example, the results displayed in Fig. 4a show that the minimum pressure-head value observed for the case using LDPE–LDPE sub-short sections is $\Delta h^{\text{LDPE-LDPE}}_{\text{min}} = 29.68$ m at $t = 2.52$ s; however, lower values are observed in the case employing LDPE–LDPE sub-short sections ($\Delta h^{\text{HDPE-LDPE}}_{\text{min}} = 20.78$ mat $t = 1.68$ s). Consequently, this particular setup of the dual technique (i.e., employing LDPE–LDPE sub-short sections) is considered for subsequent investigations.

Incidentally, the above result interpretations revealed another remarkable feature concerning the period of wave oscillations. Specifically, the forgoing observations indicate that the period spread-out involved by the dual technique is less important than that involved by the conventional technique for identical (sub-) short-section material and dimension. This shift is due to the relationship between the retardation time, which increases with time, and the period of wave oscillations.

To address closely the latter physical process, the reservoir-pipe-valve system used for numerical validation is reconsidered in the following.

Figure 5 displays the downstream pressure heads versus time predicted for HDPE piping systems for two lengths: $L = 270$ m and $L/2 = 135$ m. Figure 5 (zoomed panel) illustrates that the period of wave oscillations for the piping system length: $L = 271.8$ m, is equal to $T_{|L=271.8\,\text{m}} = 2.9613$ s; however, the corresponding period value involved by the half piping system length (i.e., $L/2 = 135.9$ m) is equal to $T_{|L/2=135.9\,\text{m}} = 1.4751$ s, which is lower than $T_{|L=271.8\,\text{m}}/2 = 1.4806$ s. This result proves that for the polymeric pipe-wall material cases the period of wave oscillation is not proportional to the piping system length. Consequently, it may be deduced that the dual technique allows limitation of spreading of the period of wave oscillations.

Hitherto, the presented analysis results are based on specific dual sub-short-section diameter and length values (i.e., $l^{\text{dual}}_{\text{sub-shortsection}} = 2.5$ m and $d^{\text{dual}}_{\text{sub-shortsection}} = 50.6$ mm). It is therefore interesting to explore the interdependencies between the damping rates of maximum pressure head, circumferential stress and radial strain (from one side), and the size of the employed sub-short sections (from the other side).

For completeness, the behavioral traces of the first peak magnitudes of downstream pressure heads, circumferential stresses and radial strains, along with the period value of the first cycle of wave oscillation, versus the up- and downstream LDPE sub-short-sections diameter and length, are illustrated in Fig. 6a, b, respectively. In particular, the following sets of sub-short-section lengths and diameters are considered: $d_{\text{sub-short-section}} = \{0.025; 0.0506; 0.075 \text{ and } 0.1\ \text{m}\}$ and $l_{\text{sub-short-section}} = \{1; 2.5; 3.5; 5; 7.5 \text{ and } 10\ \text{m}\}$, respectively. It is noteworthy that the parametric study carried out herein was based on varying only one parameter (i.e., length or diameter) of the up- or downstream short-section.

Results show that first pressure-head and circumferential-stress values decrease significantly with the increase in the applied downstream sub-short-section length for the {1; 2.5 m} values range. Contrarily, the radial strain peaks and the period value of the first cycle of wave oscillation increase with the downstream

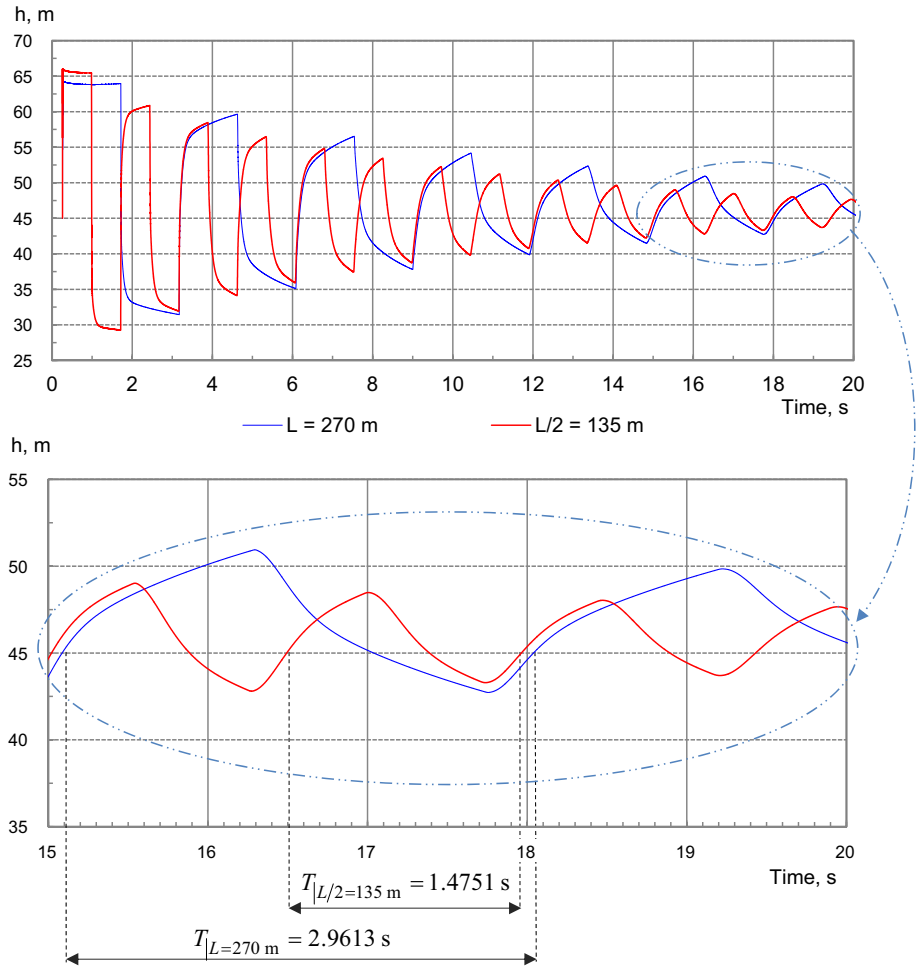

Fig. 5 Comparison of pressure heads computed at the downstream valve section for HDPE piping system lengths: $L = 270$ m and $L/2 = 135$ m

sub-short-section increase. Nonetheless, the foregoing two effects are much less visible beyond the length value sub-short-section$^{\text{downstream}} = 2.5$ m.

Also, a similar effect is observed with respect to the downstream sub-short-section diameter; however, no valuable damping is displayed beyond the diameter value $d^{\text{downstream}}_{\text{sub-short-section}} = 0.0506$ m.

On the other hand, Fig. 6a, b reveals that no valuable sensitivity of wave peaks is observed for the variation of upstream sub-short-section length and diameters.

From the foregoing result interpretations, the set of values $\{l^{\text{downstream}}_{\text{sub-short-section}} = 2.5$ m and $d^{\text{downstream}}_{\text{sub-short-section}} = 0.0506$ m$\}$ may be considered as the near-optimal values for the up- and downstream sub-short-section length and diameter.

5.2 Water-hammer downsurge event case

The purpose of this subsection is to further assess the reliability of the proposed dual-technique-based inline strategy with respect to the downsurge scenario including cavitating flow onset. Accordingly, the cavitating flow test case, performed by Bergant and Simpson [4], is selected in this subsection. The test case apparatus (Fig. 7a) is composed of a sloping piping system connecting two pressurized tanks. The main steel-pipeline specifications are: length: $L = 100$ m; internal diameter: $D = 50.6$ mm; pipe-wall thickness: $e = 3.35$ mm and elastic wave speed: $a_0 = 1369.7$ m/s. The downstream pipe axis is taken as the horizontal datum level (i.e., at elevation $z_d = 0$ m), and the upstream reservoir level is $z_u = 2.03$ m. The gauge saturated pressure head of the liquid is $h_g = -10.29$ m. As reported by these authors, the cavitating flow onset is produced by

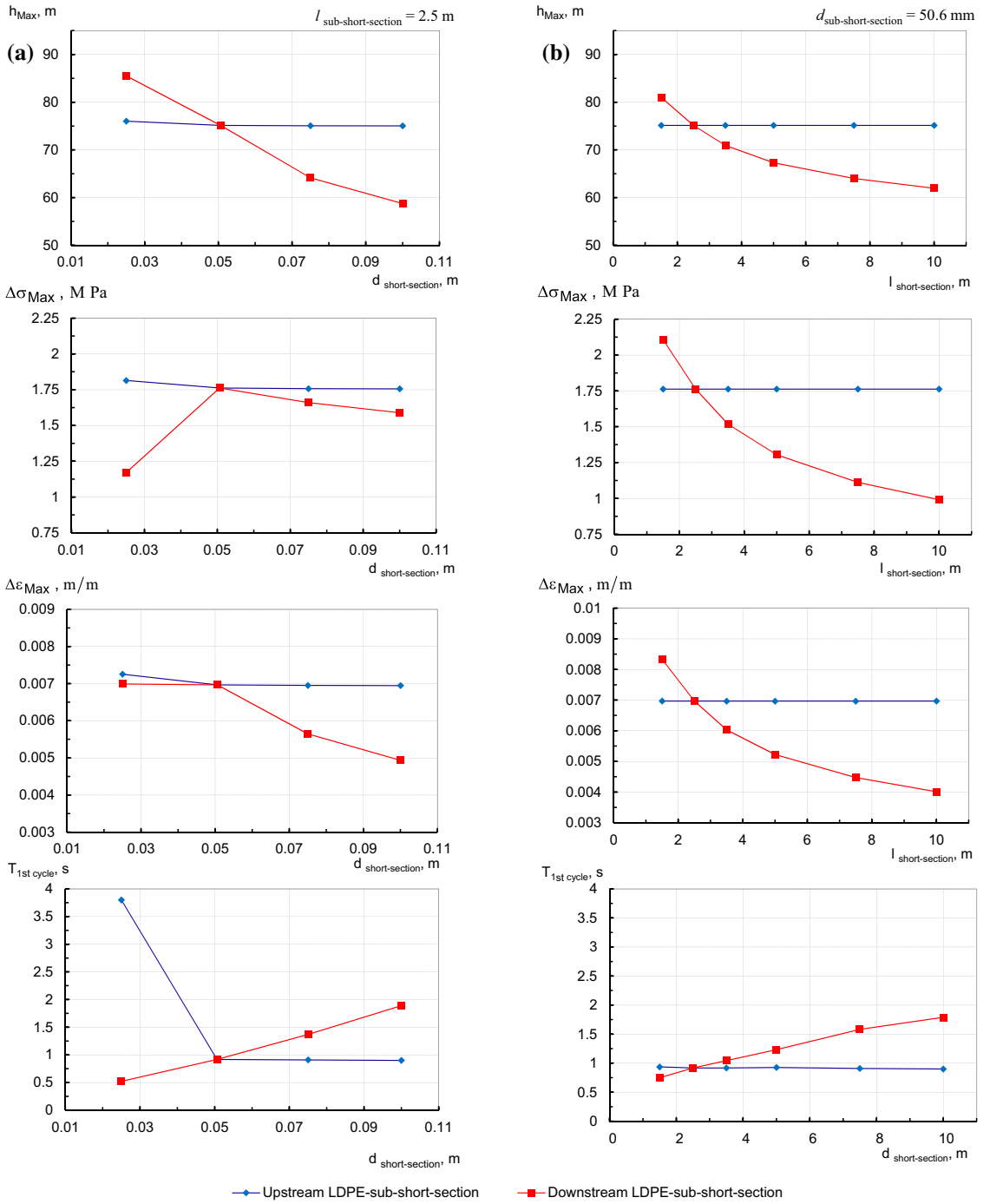

Fig. 6 Variations of maximum downstream pressure head, circumferential stress, and radial strain along with the period of the first cycle of wave oscillations as a function of the up- and downstream sub-short sections: **a** diameter (for $l_{\text{sub-short-section}} = 2.5$ m), **b** length (for $d_{\text{sub-short-section}} = 50.6$ mm)

the instantaneous and full switch-off of all flows at the upstream extremity of the steel piping system after a steady-state flow regime established for a flow velocity and a pressure head in downstream pressurized tank set constant equal to: $V_0 = 0.3$ m/s and $h_0^{T_2} = 21.4$ m, respectively. Such a transient scenario may be described by the following boundary conditions:

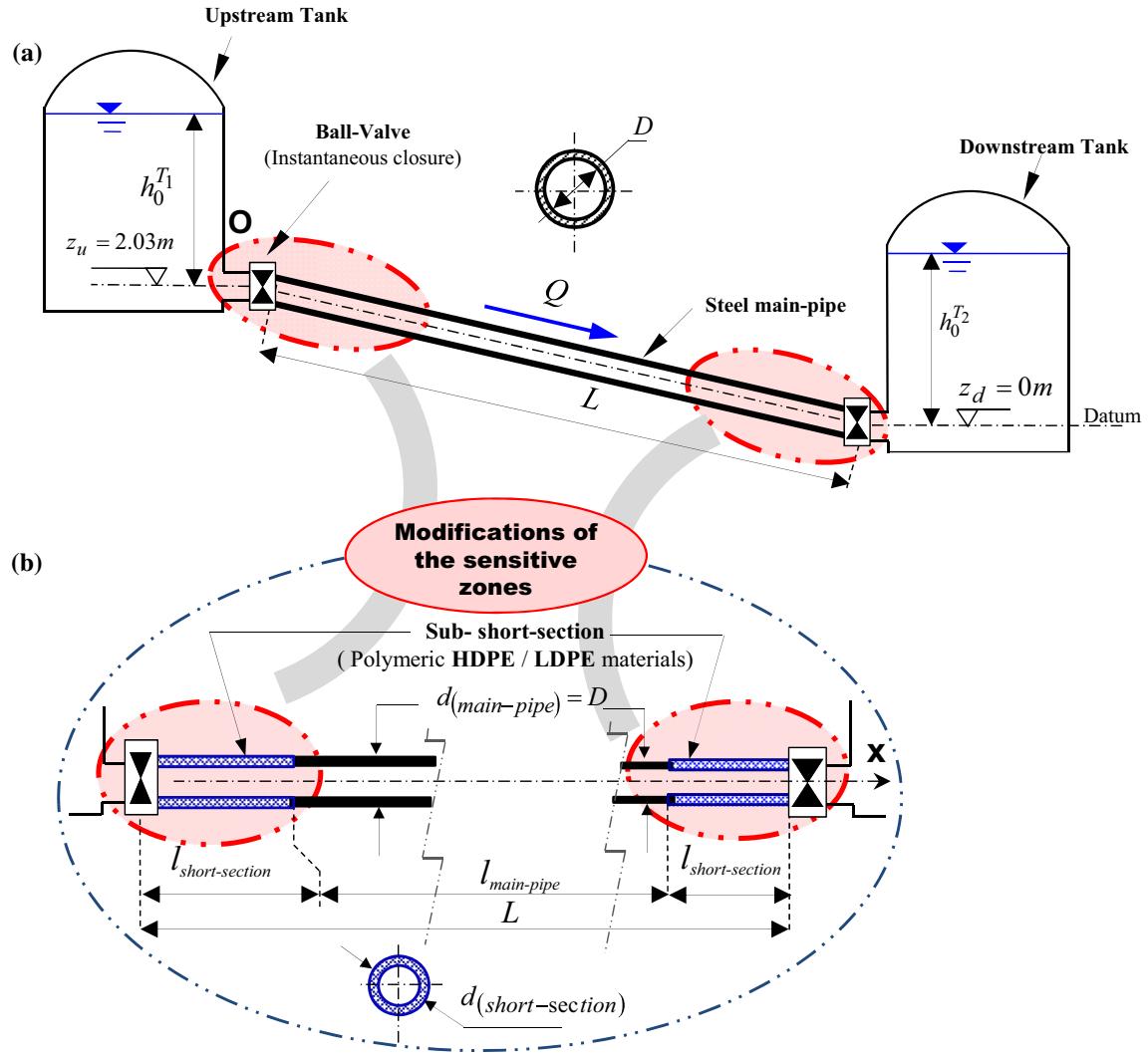

Fig. 7 Schematic layouts of: **a** primitive (non-controlled) system; **b** controlled system using the dual-technique-based inline strategy, for the downsurge control test case

$$q_{|x=0} = 0 \quad \text{and} \quad h_{|x=L} = h_0^{T_2} (t \succ 0), \tag{11}$$

For this transient situation, the dual technique consists in replacing an up- and downstream short-section of the primitive main steel pipeline by a polymeric one (HDPE or LDPE) (Fig. 7b), whereas the conventional technique handles only the upstream extremity of the primitive piping system using the same procedure.

Preliminary results are then addressed for short-section length and diameter values, used in the conventional technique, $l^{\text{conventional}}_{\text{short-section}} = 10$ m and $d^{\text{conventional}}_{\text{short-section}} (= D) = 50.6$ mm, respectively. Consequently, as for the upsurge frame, the sub-short-sections length and diameter, corresponding to the implementation of the dual technique, are: $l^{\text{dual}}_{\text{sub-shortsection}} = \left(l^{\text{conventional}}_{\text{short-section}}/2\right) = 5$ m and $d^{\text{dual}}_{\text{short-section}} (= D) = 50.6$ mm, respectively. It is worth delineating, herein, that the remaining steel piping system length, ensuing the implementation of the dual or the conventional techniques, is reduced to: $l_{\text{main-pipe}} \left(= L - l^{\text{conventional}}_{\text{short-section}} = L - 2 \times l^{\text{dual}}_{\text{sub-shortsection}}\right) = 90$ m.

The next numerical computations are performed using the MOC algorithm for a specified time-step value: $\Delta t = 0.0131$ s; a set of Courant number values: $c_r = \{0.9369; 0.6758; 1\}$, associated with the spatial discretization of the main steel pipe, along with the HDPE and LDPE sub-short sections, respectively, and a weighting factor: $\psi = 0.5$, used for the DGCM procedure.

Similarly to the previous subsection, the results for the numerical test studied herein are further detailed and substantiated in Fig. 8a–c and Table 3a–d. With reference to this data set, the following observations may be addressed for the first cycle of wave oscillations:

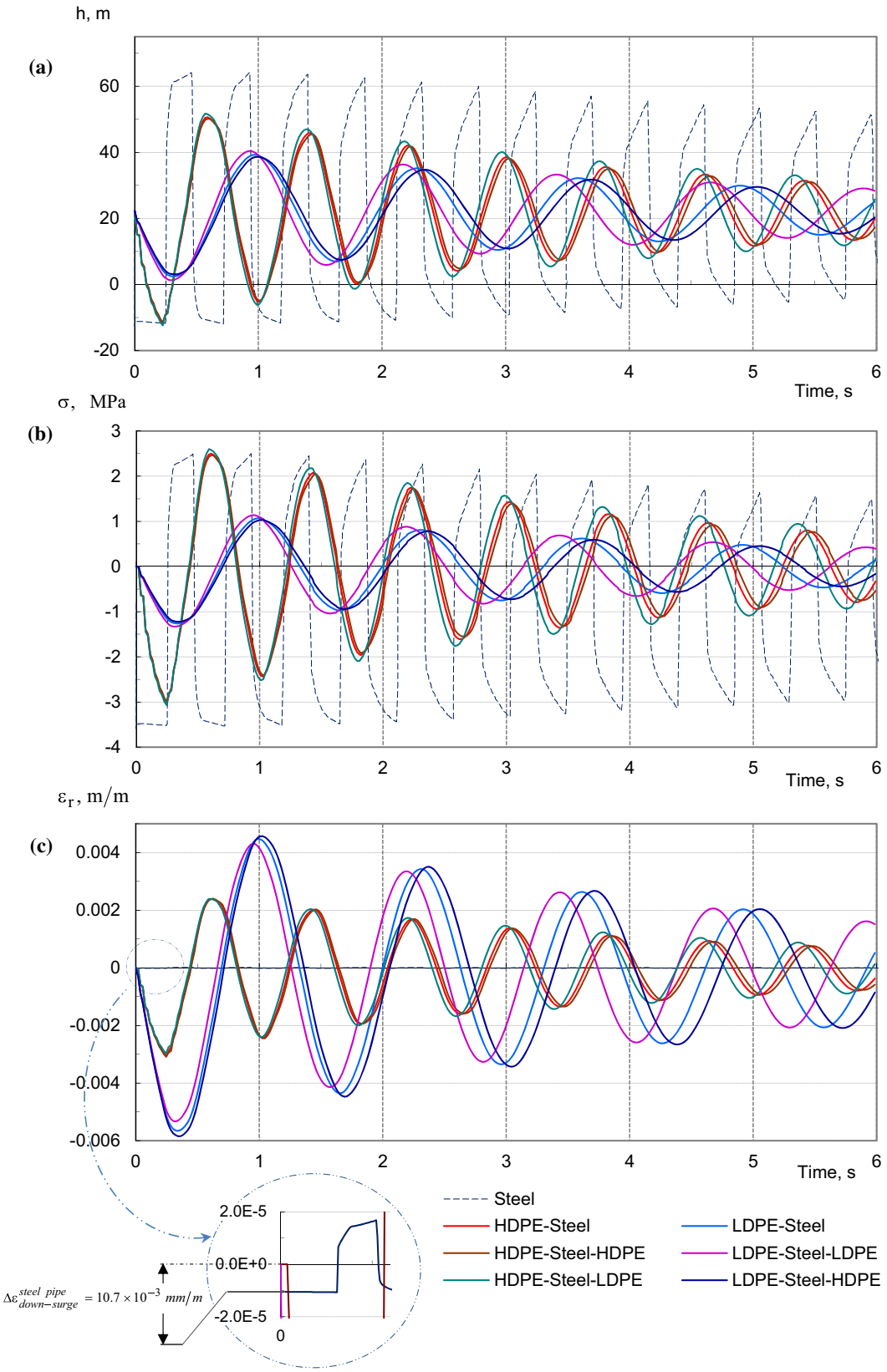

Fig. 8 Comparison of upstream **a** pressure heads, **b** circumferential stresses, and **c** radial strains versus time for the hydraulic system with and without implementation of the protection procedure

Table 3 Summary of first cycle water-hammer wave characteristics in Fig. 8

Parameters		Steel main pipe (non-controlled system)	Upstream short section (conventional technique)		Up- and downstream sub-short sections (dual technique)			
			HDPE	LDPE	HDPE–HDPE	LDPE–LDPE	HDPE–LDPE	LDPE–HDPE
(a) Pressure heads								
h_{max}	(m)	64.2	50.2	38.9	49.9	40.1	51.3	38.3
h_{min}	(m)	− 10.2	− 10.2	2.8	− 10.2	1.6	− 11.1	3.3
$\Delta h_{upsurge}$	(m)	41.8	27.9	16.5	27.5	17.7	29.0	16.0
$\delta h_{up\text{-}surge}$	(m)	–	14.0	25.3	14.3	24.1	12.9	25.9
$\delta' h_{up\text{-}surge}$	(m)	–	–	–	0.3	10.2	− 1.1	11.9
$\delta'' h_{up\text{-}surge}$	(m)	–	–	–	− 11.0	− 1.2	− 12.4	0.6
$\eta h_{up\text{-}surge}$	(%)	–	0.33	0.60	0.34	0.58	0.31	0.62
$\eta' h_{up\text{-}surge}$	(%)	–	–	–	1.22	36.51	− 3.89	42.72
$\eta'' h_{up\text{-}surge}$	(%)	–	–	–	− 66.43	− 6.98	− 75.04	3.49
$\Delta h_{downsurge}$	(m)	32.6	32.6	19.6	32.6	20.7	33.5	19.0
$\delta h_{down\text{-}surge}$	(m)	–	0.00	12.98	0.00	11.85	− 0.91	13.51
$\delta' h_{down\text{-}surge}$	(m)	–	–	–	0.00	1.65	− 0.91	13.51
$\delta'' h_{down\text{-}surge}$	(m)	–	–	–	− 12.98	− 1.14	− 13.89	0.53
$\eta h_{down\text{-}surge}$	(%)	–	0.00	39.86	0.00	36.00	28.01	41.50
$\eta' h_{down\text{-}surge}$	(%)	–	–	–	0.00	50.52	28.01	41.50
$\eta'' h_{down\text{-}surge}$	(%)	–	–	–	66.29	5.80	70.95	27.22
(b) Circumferential-stress								
$\Delta\sigma_{up\text{-}surge}$	(MPa)	2.50	2.21	1.31	2.18	1.40	2.30	1.27
$\Delta\sigma_{down\text{-}surge}$	(MPa)	3.59	2.61	1.55	2.58	1.64	2.65	1.51
$\delta\sigma_{down\text{-}surge}$	(MPa)		0.98	2.04	1.01	1.95	0.93	2.08
$\delta'\sigma_{down\text{-}surge}$	(MPa)	–	–	–	0.03	0.97	− 0.05	1.10
$\delta''\sigma_{down\text{-}surge}$	(MPa)	–	–	–	− 1.03	− 0.09	− 1.10	0.04
$\eta\sigma_{down\text{-}surge}$	(%)	–	27.32	56.75	28.04	54.25	26.06	57.94
$\eta'\sigma_{down\text{-}surge}$	(%)	–	–	–	0.99	37.05	− 1.73	42.12
$\eta''\sigma_{down\text{-}surge}$	(%)	–	–	–	− 66.39	− 5.79	− 70.96	2.74
(c) Radial strain								
$\Delta\varepsilon_{up\text{-}surge}$	(mm/m)	12.14×10^{-3}	10.72	6.37	10.59	6.81	11.14	6.14
$\Delta\varepsilon_{down\text{-}surge}$	(mm/m)	17.41×10^{-3}	12.65	7.53	12.53	7.96	12.87	7.32
$\delta\varepsilon_{down\text{-}surge}$	(mm/m)	–	− 4.76	− 9.88	− 4.88	− 9.44	− 4.54	− 10.09
$\delta'\varepsilon_{down\text{-}surge}$	(mm/m)	–	–	–	0.13	4.69	− 0.22	5.33
$\delta''\varepsilon_{down\text{-}surge}$	(mm/m)	–	–	–	− 5.00	− 0.44	− 5.34	0.21
$\eta'\varepsilon_{down\text{-}surge}$	(%)	–	–	–	0.99	37.05	− 1.73	42.12
$\eta''\varepsilon_{down\text{-}surge}$	(%)	–	–	–	− 66.39	− 5.79	− 70.96	2.74
(d) Period								
T	(s)	0.472	0.798	1.31	0.817	1.235	0.798	1.34
δT	(s)	–	0.326	0.838	0.345	0.763	0.326	0.868
$\delta' T$	(s)	–	–	0.512	0.019	0.437	0	0.437
$\delta'' T$	(s)	–	–	–	0.493	0.075	0.512	0.03

Firstly, the wave profiles of Fig. 8 may be ranked into three main wave pattern groups, corresponding to: (i) the primitive system (dashed curve); (ii) the controlled system using HDPE conventional technique; HDPE–HDPE or HDPE–LDPE dual technique (brown, red or green solid lines, respectively); and (iii) the controlled systems using LDPE conventional technique, LDPE–HDPE or LDPE–LDPE dual technique (pink, blue or navy blue solid lines, respectively).

Secondly, Fig. 8a reveals the cavitating flow incidence throughout the primitive system case, succeeding the upstream valve closure. For instance, basing on Fig. 8a together with Table 3a, the pressure head first falls to the gauge value $h_{min} = -10.2$ m and then rises to a maximum peak value ($h_{max} = 64.2$ m). In other words, the magnitude values of pressure-head drop and rise, computed referring to the initial steady-state benchmark, are $\Delta h^{\text{steel-pipe}}_{\text{down-surge}} = 32.6$ m and $\Delta h^{\text{steel-pipe}}_{\text{up-surge}} = 41.8$ m, respectively. On the other hand, concerning the upstream circumferential-stress pattern of Fig. 8b (and Table 3b), the magnitudes of upstream circumferential-stress drop and rise are: $\Delta\sigma^{\text{steel-pipe}}_{\text{down-surge}} = 3.59$ MPa and $\Delta\sigma^{\text{steel-pipe}}_{\text{up-surge}} = 2.5$ MPa, respectively. Likewise, the corresponding magnitudes of upstream radial strain drop and rise, Fig. 8c (and Table 3c), are: $\Delta\varepsilon^{\text{steel-pipe}}_{\text{down-surge}} = 17.41$ μm/m and $\Delta\varepsilon^{\text{steel-pipe}}_{\text{up-surge}} = 12.14$ μm/m, respectively.

A similar assessment may be addressed to the second group of the controlled system. Indeed, the controlled system cases based on HDPE conventional technique, HDPE–HDPE or HDPE–LDPE dual-technique setups

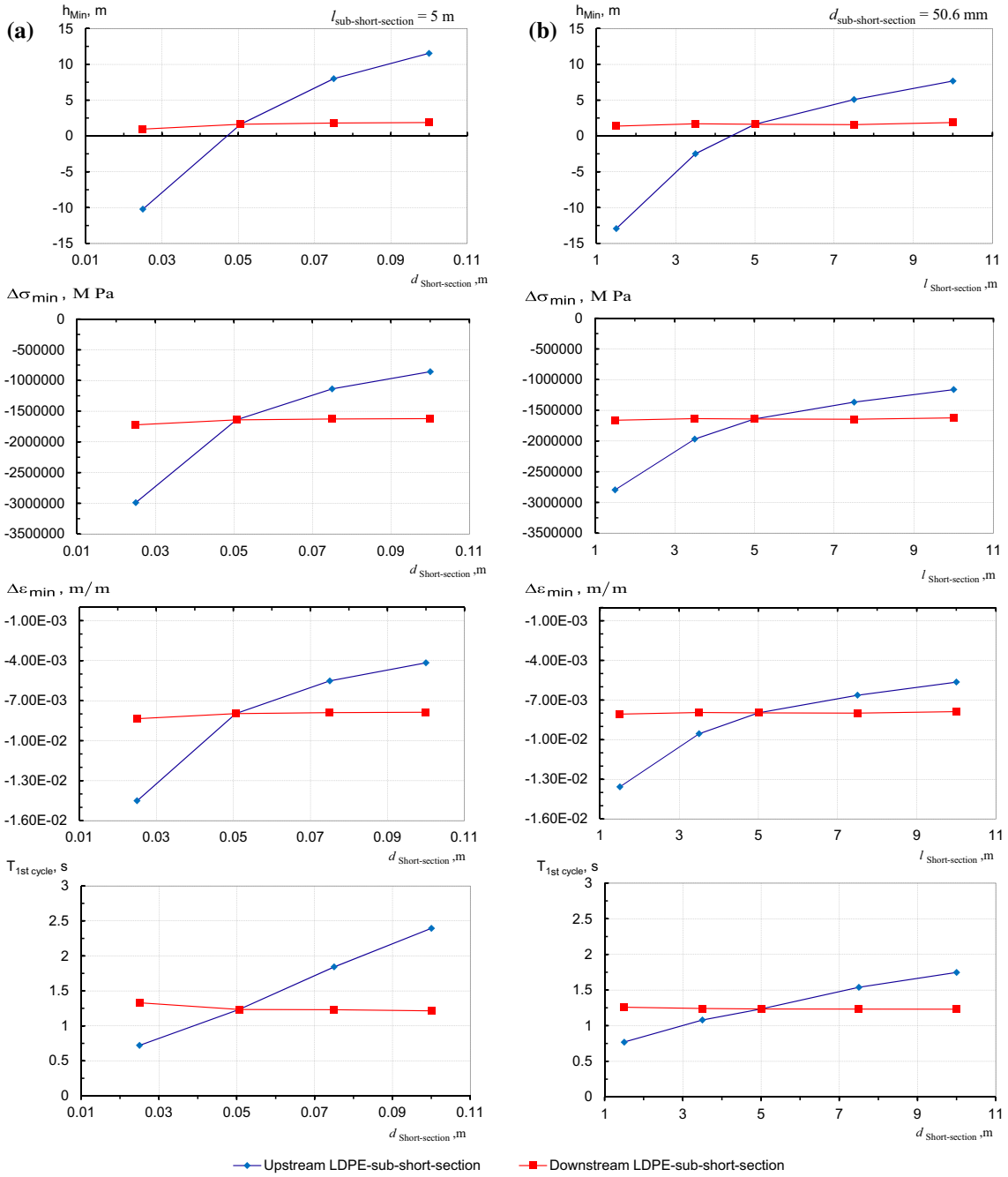

Fig. 9 Variations of minimum upstream pressure head, circumferential stress, and radial strain along with the period of the first cycle of wave oscillations as functions of the up- and downstream sub-short sections: **a** diameter (for $l_{\text{sub-short-section}} = 5$ m), **b** length (for $d_{\text{sub-short-section}} = 50.6$ mm)

have no contribution in terms of attenuation of severe pressure-head drop limitation. Perhaps, these controlled system configurations allow the damping of the upsurge rather than the downsurge.

Nonetheless, Fig. 8 proves that the cavitating flow regime may be avoided if the hydraulic system is controlled using the LDPE conventional technique, the LDPE–HDPE or the LDPE–LDPE dual technique (third wave pattern group). For instance, Fig. 8a (and Table 3a) illustrates a low pressure-head drop magnitude associated with this wave pattern group: $\Delta h^{\text{LDPE}}_{\text{down-surge}} = 19.6$ m, $\Delta h^{\text{LDPE-HDPE}}_{\text{down-surge}} = 19.0$ m or $\Delta h^{\text{LDPE-LDPE}}_{\text{down-surge}} = 20.7$ m, corresponding to the LDPE conventional technique, LDPE–HDPE or LDPE–LDPE

dual techniques, respectively. Particularly, these configurations of the controlled systems allow a significant amortization of the downsurge pressure head compared with those observed within the primitive hydraulic system: $\delta h^{\text{LDPE}}_{\text{down-surge}} = 12.98$ m $\delta h^{\text{LDPE-HDPE}}_{\text{down-surge}} = 13.51$ m or $\delta h^{\text{LDPE-LDPE}}_{\text{down-surge}} = 11.85$ m. In return, the amortization rates of the pressure-head drop associated with LDPE conventional technique, LDPE–HDPE or LDPE–LDPE dual techniques, are equal to $\eta^{\text{LDPE}}_{\text{down-surge}} = 39.86\%$, $\eta^{\text{LDPE-HDPE}}_{\text{down-surge}} = 41.50\%$ or $\eta^{\text{LDPE-LDPE}}_{\text{down-surge}} = 36.00\%$, respectively.

However, an preliminary observations indicate about similar efficiencies of the foregoing controlled system setups, in terms of downsurge attenuation; a noteworthy comment should be emphasized with regard to the period of wave oscillation cycles involved by each setup. Thereupon, detailed examination of Fig. 8 (and Table 3d) shows that the best wave pattern is perhaps that involved by the LDPE–LDPE dual technique; this deduction is more evident for the subsequent cycles of wave oscillations. Precisely, the latter particular dual-technique setup induces a spreading out of the period of wave oscillations equal to: $\delta T^{\text{LDPE-LDPE}}_{\text{1stcycle}} = 0.763$ s compared with those associated with the primitive system. Similarly, a lower period spread-out is involved by the LDPE–LDPE dual technique compared with the HDPE conventional technique ($\delta' T^{\text{LDPE-LDPE}}_{\text{1stcycle}} = 0.437$ s). However, the LDPE–LDPE dual-technique configuration lessened the period spread-out depicted throughout the controlled system employing an LDPE conventional technique ($\delta'' T^{\text{LDPE-LDPE}}_{\text{1st cycle}} = 0.075$ s).

Additional benefit arising from the implementation of the LDPE–LDPE dual-technique-based inline strategy concerns the limitation of excessive radial-strain amplification induced by the conventional techniques. Indeed, Fig. 8 (and Table 3c) indicates that the latter dual technique lowered the radial-strain amplification rate involved by the LDPE conventional technique (i.e., $\delta'' \varepsilon^{\text{LDPE-LDPE}}_{\text{up-surge}} = 0.44$ mm/m). However, this technique augmented the radial-strain amplification as compared with the HDPE-based conventional technique (i.e., $\delta' \varepsilon^{\text{LDPE-LDPE}}_{\text{up-surge}} = 4.69$ mm/m).

Incidentally, it is noteworthy that the LDPE–LDPE dual technique, discussed above, provides also much more upsurge attenuation of pressure head and circumferential stress than those associated with the HDPE conventional-technique-based controlled system (i.e., $\delta' h^{\text{LDPE-LDPE}}_{\text{up-surge}} = 10.2$ m and $\delta' \sigma^{\text{LDPE-LDPE}}_{\text{up-surge}} = 0.97$ MPa). However, the former technique slightly lessens the pressure-head attenuation provided by the LDPE conventional technique ($\delta'' h^{\text{LDPE-LDPE}}_{\text{up-surge}} = 6.98$ m and $\delta'' \sigma^{\text{LDPE-LDPE}}_{\text{up-surge}} = 0.09$ MPa).

However, an inverse analysis may be conducted with respect to the radial-strain pattern plotted in Fig. 8c. Indeed, similar comparisons indicate that the LDPE–LDPE dual technique discussed above leads to an amplification of radial-strain upsurge equal to $\delta' \varepsilon^{\text{LDPE-LDPE}}_{\text{up-surge}} = 4.36$ mm/m as compared with the HDPE conventional technique, and an even more important amplification (or $\delta'' \varepsilon^{\text{LDPE-LDPE}}_{\text{up-surge}} = 4.69$ mm/m) as compared with the LDPE conventional technique. Incidentally, a very small upsurge magnitude of radial strain is observed for the this case $\Delta \varepsilon^{\text{steel-pipe}}_{\text{up-surge}} = 12.14$ μm/m (zoomed panel of Fig. 8c).

From the above discussions, as for the upsurge control case, it is believed that the LDPE–LDPE setups of the dual technique provide a satisfactory trade-off between the damping of pressure head and circumferential stress from one side, and the limitation of period spread-out and radial-strain amplification from the other side. Consequently, as for the upsurge case, the following investigation would deal with this particular setup of the dual technique.

Similarly to the upsurge case, the sensitivity analysis of the first peaks magnitude of upstream pressure heads, circumferential stresses and radial strains, along with the period of wave oscillation versus the sub-short-section diameter and length computed across the controlled system based on the LDPE–LDPE dual technique, is illustrated in Fig. 9a, b, respectively. Specifically, the following sets of lengths and diameters are performed: $d_{\text{sub-short-section}} = \{0.025\,; 0.0506; 0.075 \text{ and } 0.1 \text{ m}\}$ and $l_{\text{sub-short-section}} = \{1\,; 2.5; 7.5 \text{ and } 10 \text{ m}\}$, respectively.

First, results show that the reduction in pressure peak magnitude is principally driven by an increase in upstream sub-short-section length and diameter. Second, small damping (or amplification) effects associated with pressure head and circumferential stress (or period of wave oscillation and radial strain) are observed beyond the sub-short-section length and diameter $\left\{l^{\text{downstream}}_{\text{sub-short-section}} = 2.5\,\text{m} \text{ and } d^{\text{downstream}}_{\text{sub-short-section}} = 0.0506\,\text{m}\right\}$. Thus, the foregoing values may be considered as the near- optimal values for the up- and downstream sub-short-section length and diameter.

6 Conclusions

To sum up, the merits of the proposed dual-technique-based inline strategy may be enumerated as follows:

(i) The dual-technique implementation resulted in a significant reduction in pressure head and circumferential stress and identified an even better alternative than the conventional-technique-based inline strategy in terms of limitation of period spread-out and radial-strain amplification.
(ii) The particular dual-technique setup using an up- and downstream LDPE sub-short section has proven to be the better setup providing an acceptable trade-off between the aforementioned criteria.
(iii) The parametric study of pressure-head, circumferential-stress and radial-strain peak (or crest) values with respect to the sub-short-section length and diameter identified the near-optimal value for dimensioning the compound short section.

One considers that such a dual technique is suggested to enhance the reliability and improve the cost-effectiveness design of hydraulic utilities, while providing inherently free maintenance and/or testing benefits compared with conventional surge control devices.

Though the dual-technique-based inline control strategy is numerically tested on a single pipeline system, experimental investigations on the presented strategy may be considered as motivating research perspectives of this study.

References

1. Abbasi, A., Sabbagh-Yazdi, S.R., Wegian, F.M.: Accurate water hammer pressure modeling for automatic modification of circumferential-stress distribution along multi-segment pipelines. Water Sci. Technol. Water Suppl. WSTWS **9**(3), 269–278 (2009)
2. Adamkowski, A., Lewandowski, M.: Investigation of hydraulic transients in a pipeline with column separation. J. Hydraul. Eng. **138**(11), 935–944 (2012)
3. Aklonis, J.J., MacKnight, W.J., Shen, M.: Introduction to Polymer Viscoelasticity. Wiley, New York (1972)
4. Bergant, A., Simpson, A.: Pipeline column separation flow regimes. J. Hydraul. Eng. ASCE **125**, 835–848 (1999). https://doi.org/10.1061/(ASCE)0733-9429
5. Bergant, A., Simpson, A.R., Tijsseling, A.: Water-hammer with column separation: a historical review. J. Fluids Struct. **22**(2), 135–171 (2006)
6. Boulos, P.F., Karney, B.W., Wood, D.J., Lingireddy, S.: Hydraulic transient guidelines for protecting water distribution systems. Am. Water Works Assoc. **97**(5), 111–124 (2005)
7. Brinson, H.F., Brinson, L.C.: Polymer Engineering Science and Viscoelasticity: An Introduction. Springer, New York (2008)
8. Covas, D., Stoianov, I., Ramos, H., Graham, N., Maksimovic, C., Butler, D.: Water-hammer in pressurized polyethylene pipes: conceptual model and experimental analysis. Urban Water J. **1**(2), 177–197 (2004)
9. Covas, D., Stoianov, I., Ramos, H., Graham, N., Maksimovic, C.: The dynamic effect of pipe-wall viscoelasticity in hydraulic transients. Part I-experimental analysis and creep characterization. J. Hydraul. Res. **42**(5), 517–532 (2004)
10. Covas, D., Stoianov, I., Mano, J.F., Ramos, H., Graham, N., Maksimovic, C.: The dynamic effect of pipe-wall viscoelasticity in hydraulic transients. Part II-model development, calibration and verification. J. Hydraul. Res. **43**(1), 56–70 (2005). https://doi.org/10.1080/00221680509500111
11. Ghidaoui, M., Karney, B.: Equivalent differential equations in fixed-grid characteristics method. J. Hydraul. Eng. **120**(10), 1159–1175 (1994)
12. Ghidaoui, M.S., Zhao, M., Duncan, A.M., David, H.A.: A review of water-hammer theory and practice. Appl. Mech. Rev. **58**, 49–76 (2005)
13. Güney, M.S.: Water-hammer in viscoelastic pipes where cross-section parameters are time dependent. In: Proceedings of the 4th International Conference on Pressure Surges, BHRA, Bath, pp. 189–209 (1983)
14. Kim, S.-G., Lee, K.-B., Kim, K.-Y.: Water hammer in the pump-rising pipeline system with an air chamber. J. Hydrodyn. **26**(6), 960–964 (2015)
15. Massouh, F., Comolet, R.: Étude d'un système anti-bélier en ligne-study of a water-hammer protection system in line. La Houille Blanche **5**, 355–362 (1984)
16. Pejovic, S., Boldy, A.P., Obradovic, D.: Guidelines to Hydraulic Transient Analysis. Technical Press, Brookfield (1987)
17. Pothof, I., Karney, B.: Guidelines for transient analysis in water transmission and distribution systems. Water Supply System Analysis (InTech) (2012)
18. Pezzinga, G.: Evaluation of time evolution of mechanical parameters of polymeric pipes by unsteady flow runs. J. Hydraul. Eng. ASCE **140**(12), 04014057 (2014)
19. Sadafi, M.H., Riasi, A., Raisee, M., Nourbakhsh, A.: Cavitating flow during water-hammer using a generalized interface vaporous cavitation model. J. Fluids Struct. **34**, 190–201 (2012)
20. Soares, A., Covas, D., Reis, L.: Analysis of PVC pipe-wall viscoelasticity during water-hammer. J. Hydraul. Eng. **134**(9), 1389–1394 (2008)
21. Soares, A., Covas, D., Carriço, N.: Transient vaporous cavitation in viscoelastic pipes. J. Hydraul. Res. **50**(2), 228–235 (2012). https://doi.org/10.1080/00221686.2012.669143
22. Triki, A.: Multiple-grid finite element solution of the shallow water equations: water-hammer phenomenon. Comput. Fluids **90**, 65–71 (2014)

23. Triki, A.: Waterhammer control in pressurized-pipe flow using an in-line polymeric short-section. Acta Mech. **227**(3), 777–793 (2016). https://doi.org/10.1007/s00707-015-1493-13
24. Triki, A.: Water-hammer control in pressurized-pipe flow using a branched polymeric penstock. J. Pipeline Syst. Eng. Pract. ASCE **8**(4), 04017024 (2017a). https://doi.org/10.1061/(ASCE)PS.1949-1204.0000277
25. Triki, A.: Further investigation on water-hammer control inline strategy in water-supply systems. J. Water Suppl. Res. Technol. AQUA (2017b). https://doi.org/10.2166/aqua.2017.073
26. Vitkovsky, J.P., Lambert, M.F., Simpson, A.R., Bergant, A.: Advances in unsteady friction modelling in transient pipe flow. In: The 8th International Conference on Pressure Surges, BHR, The Hague, The Netherlands (2000)
27. Wan, W., Huang, W., Li, C.: Sensitivity analysis for the resistance on the performance of a pressure vessel for water hammer protection. J. Pressure Vessel Technol. Trans. ASME **136**(1), Article number 011303 (2014)
28. Wan, W., Li, F.: Sensitivity analysis of operational time differences for a pump-valve system on a water hammer response. J. Pressure Vessel Technol. Trans. ASME **138**(1), Article number 011303 (2016)
29. Wood, D.J., Lingireddy, S., Boulos, P.F.: Shock and water-hammer loading. In: Pressure Vessels and Piping Systems-UNESCO-Encyclopedia Life Support Systems (EOLSS) (2005)
30. Wylie, E.B., Streeter, V.L.: Fluid Transients in Systems. Prentice Hall, Englewood Cliffs (1993)